



Kinetic water-bag model of global collisional drift waves and ion temperature gradient instabilities in cylindrical geometry

E. Gravier and E. Plaut

Citation: [Phys. Plasmas](#) **20**, 042105 (2013); doi: 10.1063/1.4799814

View online: <http://dx.doi.org/10.1063/1.4799814>

View Table of Contents: <http://pop.aip.org/resource/1/PHPAEN/v20/i4>

Published by the [American Institute of Physics](#).

Additional information on Phys. Plasmas

Journal Homepage: <http://pop.aip.org/>

Journal Information: http://pop.aip.org/about/about_the_journal

Top downloads: http://pop.aip.org/features/most_downloaded

Information for Authors: <http://pop.aip.org/authors>

ADVERTISEMENT

The advertisement banner features a background of green, wavy, fiber-like patterns. At the top, the 'AIP Advances' logo is shown, with 'AIP' in blue and 'Advances' in green, accompanied by a series of orange circles of varying sizes. Below the logo, the text 'Special Topic Section: PHYSICS OF CANCER' is displayed in white on a dark green background. At the bottom, the text 'Why cancer? Why physics?' is written in yellow, and a blue button with white text says 'View Articles Now'.

Kinetic water-bag model of global collisional drift waves and ion temperature gradient instabilities in cylindrical geometry

E. Gravier¹ and E. Plaut²

¹Institut Jean Lamour, UMR 7198 CNRS—Université de Lorraine, Bd des Aiguillettes, 54 506 Vandœuvre-lès-Nancy Cedex, France

²LEMETA, UMR 7563 CNRS—Université de Lorraine, 2, av. de la Forêt de Haye, 54 518 Vandœuvre-lès-Nancy Cedex, France

(Received 18 February 2013; accepted 20 March 2013; published online 8 April 2013)

Collisional drift waves and ion temperature gradient (ITG) instabilities are studied using a linear water-bag kinetic model [P. Morel *et al.*, Phys. Plasmas **14**, 112109 (2007)]. An efficient spectral method, already validated in the case of drift waves instabilities [E. Gravier *et al.*, Eur. Phys. J. D **67**, 7 (2013)], allows a fast solving of the global linear problem in cylindrical geometry. The comparison between the linear ITG instability properties thus computed and the ones given by the COLUMBIA experiment [R. G. Greaves *et al.*, Plasma Phys. Controlled Fusion **34**, 1253 (1992)] shows a qualitative agreement. Moreover, the transition between collisional drift waves and ITG instabilities is studied theoretically as a function of the ion temperature profile. © 2013 American Institute of Physics. [<http://dx.doi.org/10.1063/1.4799814>]

I. INTRODUCTION

Low-frequency turbulence developing from micro instabilities is responsible for the phenomenon of anomalous transport in magnetically confined fusion plasmas.^{1,2} Thus, drift waves, Ion Temperature Gradient (ITG), interchange and Trapped Electron Modes (TEM) instabilities probably play an important role in explaining the anomalous heat and particle transport observed in tokamaks.^{3,4} These instabilities are driven by gradients of the density or temperature of the ion and electron populations. Low-frequency density fluctuations are also easily observed in cylindrical magnetized plasma columns.^{5–9} These cylindrical machines are of fundamental interest and can provide a testing ground for comparisons of numerical simulations with experiments.

Numerical simulations can contribute to a better understanding of plasma instabilities. Fluid models have been widely used. Solving three-dimensional 3D fluid equations is the most convenient way to compute the plasma response to the perturbed electromagnetic field when there is no wave-particle interaction, and is all the more justified when Coulomb collisions are dominant. But predicting turbulent transport in nearly collisionless fusion plasmas may require solving gyrokinetic equations.¹⁰

On the other hand, although more accurate, the kinetic calculation of turbulent transport is much more demanding of computer resources than fluid simulations. Furthermore, solving kinetic equations is still a nontrivial task. This motivated us to revisit an alternative approach based on the water-bag (WB) representation of the distribution function.¹¹ The water bag model fills the gap between fluid and kinetic descriptions of a collisionless and unmagnetized plasma, incorporating kinetic effects, but with the complexity of a multifluid model.

Recently, we used the water bag model for magnetized plasmas in the framework of gyrokinetic modeling (Gyro-Water-Bag, i.e., GWB model) in cylindrical geometry with a

uniform and static magnetic field pointing in the axis direction. In Ref. 12, a local linear study of the ITG instability in cylindrical geometry has been performed in the case of the drift-kinetic approximation without taking into account Finite Larmor Radius (FLR) effects, polarization, and gyroaveraging. It has been shown that the water-bag model converges rather rapidly towards that of the continuous distribution function (bag number ≥ 5) when ITG instability linear growth rates are compared. Next, a linear study of both local collisional drift waves and ITG instabilities has been performed.¹³ Finally, a precise study of FLR effects on ITG instability has been presented in Ref. 14. In all these studies, the eigenfunctions were not computed exactly but approximated assuming local modes. For instance in Refs. 13 and 14, the electric potential was assumed to be of a Gaussian form, centered around a radius r_0 , see the Eqs. (23) and (31) of Ref. 13 and Eqs. (13) and (15) of Ref. 14. Here, we revisit these studies by solving systematically the eigenproblems, i.e., by performing a "global" stability analysis. For this purpose, we use the new spectral method introduced in Ref. 15.

A Gyro-Water-Bag model could be useful of course for nonlinear simulations but also for linear studies. In this frame, the Gyro-Water-Bag model could be an interesting and efficient linear tool, giving linear instability growth rates and eigenfunctions, and allowing to compare easily the linear instability growth rate with that given by nonlinear gyrokinetic codes. Also the linear model should be relevant when regular and almost sinusoidal waves are observed experimentally.

This article is organized as follows. In Sec. II, the kinetic water-bag model is introduced and the linear analysis is presented. The model is able to describe both collisional drift waves and ITG instabilities. In Sec. III, the new spectral method is presented. It will allow us to solve the differential equation given by the linear analysis. The influence of the ion temperature and kinetic effects on ITG

instabilities are discussed in Sec. IV, and a comparison with the COLUMBIA experiment^{5,6} is performed. The waves observed experimentally are nearly regular and sinusoidal. In the framework of a linear model, it is, therefore, reasonable to assume that they correspond to the fastest growing modes of the stability analysis. Finally, the transition between collisional drift waves and ITG instabilities is studied theoretically in Sec. V, with the temperature profile as the control parameter.

II. KINETIC WATER-BAG MODEL

A. Generalities—base state

We consider a cylindrical plasma of radius a . The plasma is confined by a uniform magnetic field $\mathbf{B} = B\mathbf{u}_z$, with \mathbf{u}_z the unit vector in the axial direction. The plasma can be weakly or fully ionized. Three species can be considered: the neutral gas, the electron fluid, which is free to collide and to exchange momentum with the neutral gas, and finally the ion fluid. Ion-neutral collisions are neglected. It is also assumed that fluctuations of the magnetic field are negligible. The ion and electron fluids are coupled by the quasi-neutrality equation.

When the ion thermal velocity v_{Ti} is close to the phase velocity $v_\phi = \omega/k_\parallel$, with ω the wave angular frequency and k_\parallel its parallel wavenumber, resonant interactions between waves and particles play an important role in determining the instability growth rate. Moreover, ion-neutral collisions are neglected hereafter. Consequently, a kinetic model that directly determines the distribution function is required.

Fluctuations in strongly magnetized plasmas occur on time scales much longer than charged particle gyromotion period: $\omega \ll \Omega_c$ the ion cyclotron frequency. Moreover, the ion Larmor radius is much smaller than the characteristic length scale of density gradient $n/|\nabla n|$. This gyrokinetic ordering¹⁰ allows separation between fast gyromotion and slow dynamics in the direction perpendicular to the magnetic field. The gyrokinetic model makes full use of the μ -invariance to eliminate perpendicular kinetic variables in the Vlasov equation, with $\mu = m_i v_\perp^2/2B$ the first adiabatic invariant, which is linked to the perpendicular dynamic. Thus, the phase space reduces to three dimensions in real space and one dimension in velocity space. The ions are described by the statistical distribution function $f(\mathbf{r}, v_\parallel, t)$ of their guiding-center (GC) position. The variable v_\parallel is the velocity in the direction parallel to the magnetic field. The gyrokinetic Vlasov equation reads

$$\partial_t f + \left(\frac{\mathbf{E} \times \mathbf{B}}{B^2} + v_\parallel \mathbf{u}_z \right) \cdot \nabla f + \dot{v}_\parallel \partial_{v_\parallel} f = 0 \quad (1)$$

with $\dot{v}_\parallel = qE_\parallel/m_i$, q the ionic charge, $\mathbf{E} = -\nabla J_0 \Phi$, Φ the electric potential, $J_0(k_\perp v_\perp/\Omega_c)$ the gyroaverage operator, i.e., the zero order Bessel function of the first kind in Fourier space,¹⁶ given by Eq. (15) in Ref. 17, k_\perp the perpendicular wave number, and $v_\perp \simeq v_{Ti} = \sqrt{KT_i/m_i}$, T_i the ion temperature. Here, the magnetic moment μ , or the perpendicular velocity v_\perp , is just a parameter defining different particle classes, each of them having a different Larmor radius.

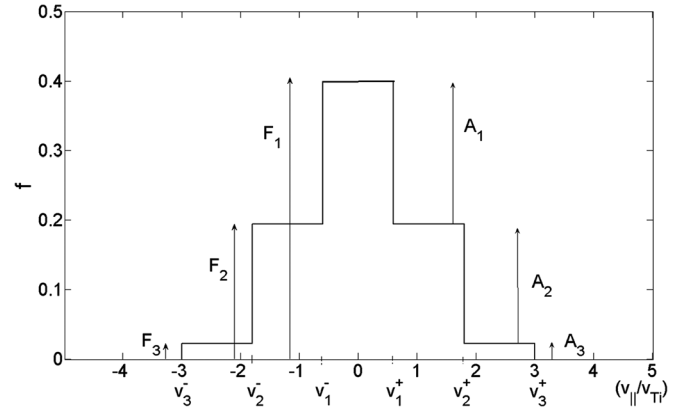


FIG. 1. Water-Bag distribution function for $M = 3$ plotted against the parallel velocity.

In the same way, the WB concept uses Liouville's invariance to reduce again the phase space dimension. A detailed presentation of the Gyro-Water-Bag model and the method for choosing water-bag parameters can be found in Refs. 12–14.

An ion distribution function of the following form (Fig. 1) is chosen:

$$f_{MWB}(\mathbf{r}, v_\parallel, t) = \sum_{j=1}^M A_j \{H[v_\parallel - v_j^-(\mathbf{r}, t)] - H[v_\parallel - v_j^+(\mathbf{r}, t)]\} \quad (2)$$

with M the bag number and H the heaviside step-function. The interesting property of the WB distribution is the absolute time invariance of the bag heights A_j . Consequently, the evolution of the system is entirely determined by the evolution of the contours $v_j^+(\mathbf{r}, t)$ and $v_j^-(\mathbf{r}, t)$ (Fig. 2). Introducing this distribution function in the gyrokinetic equation leads to the following set of equations, called contour equations:¹²

$$\partial_t v_j^\pm + \frac{\mathbf{E} \times \mathbf{B}}{B^2} \cdot \nabla_\perp v_j^\pm + v_j^\pm \nabla_\parallel v_j^\pm = \dot{v}_j^\pm = \frac{qE_\parallel}{m_i}. \quad (3)$$

These contours are coupled by the quasi-neutrality equation. The polarization drift can be explicitly introduced in

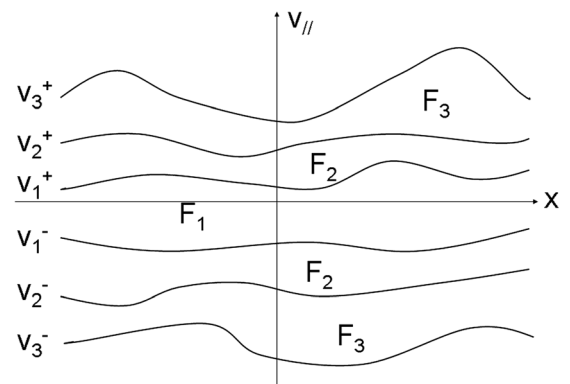


FIG. 2. Bag contours in the phase space x, v for a three-bag system. Between two contours, the distribution function f remains equal to a constant F_j . Note that Fig. 1 shows a typical profile of the function f at a particular x -value.

the Vlasov equation or can be written as a perturbed ion density,¹⁸ so that the quasi-neutrality equation reads

$$n_e = J_0 n_i + \nabla_{\perp} \cdot \left(\frac{n_i}{\Omega_e B} \nabla_{\perp} \Phi \right) \quad (4)$$

with

$$n_i = \sum_{j=1}^M A_j (v_j^+ - v_j^-). \quad (5)$$

Hereafter, we assume ions with one positive charge $q = e$. The second term in the right hand side of Eq. (4) is the polarization term.

To sum up, the use of magnetic moments and Liouville invariance yields an exact reduction of the phase space: it is now simply the physical space. The drawback is that the velocities v_{\perp} and v_{\parallel} reappear as parameters in the various magnetic moments μ and bag contours v_j^{\pm} . Since there is no mathematical lower bound on the bag number M , from a physical point of view, many interesting results can be obtained even with small values of M .¹² Note also that the GWB approach is not restricted to Maxwellian distribution functions. The sampling j allows to consider any arbitrary function of the parallel velocity v_{\parallel} .

B. Linear stability equations

Linear perturbations are assumed. Using cylindrical coordinates (r, θ, z) , the electrostatic potential of a wave is

$$\Phi(r, \theta, z, t) = \phi(r) \exp[i(m\theta + k_{\parallel}z - \omega t)] + c.c., \quad (6)$$

with m the azimuthal wavenumber, k_{\parallel} the parallel wavenumber, and ω the wave angular frequency. We will often use the notation $k_{\theta} = m/r$. Similarly, the densities

$$n_i = n_0(r) + n_{i1}(r) \exp[i(m\theta + k_{\parallel}z - \omega t)] + c.c., \quad (7)$$

$$n_e = n_0(r) + n_{e1}(r) \exp[i(m\theta + k_{\parallel}z - \omega t)] + c.c., \quad (8)$$

and the velocities

$$v_j^{\pm} = \pm a_j(r) + W_j^{\pm}(r) \exp[i(m\theta + k_{\parallel}z - \omega t)] + c.c., \quad (9)$$

with a_j the velocity of the j th bag at equilibrium, i.e., $v_j^+ = a_j$ and $v_j^- = -a_j$ at equilibrium.

By linearizing Eq. (3), one obtains

$$W_j^{\pm} = \frac{k_{\parallel} q / m_i \mp (k_{\theta} / B) \partial a_j / \partial r}{\omega \mp k_{\parallel} a_j} J_0 \phi. \quad (10)$$

Noticing that, according to Eq. (5),

$$n_{i1} = \sum_{j=1}^M A_j (W_j^+ - W_j^-), \quad (11)$$

by linearizing the right hand side of Eq. (4), one obtains

$$n_{e1} = \frac{n_0 q}{KT_e} J_0^2 \phi \sum_{j=1}^M \alpha_j \frac{k_{\parallel}^2 c_s^2 - \frac{1}{\tau} \omega \Omega_j^*}{\omega^2 - k_{\parallel}^2 a_j^2} + \frac{n_0}{\Omega_e B} \left[\frac{d^2 \phi}{dr^2} + \left(\kappa_n + \frac{1}{r} \right) \frac{d\phi}{dr} - k_{\theta}^2 \phi \right] \quad (12)$$

with T_e the electron temperature

$$\Omega_j^* = \frac{KT_i}{qB} k_{\theta} \partial_r \ln a_j, \quad (13)$$

$$\alpha_j = 2a_j A_j / n_0, \quad (14)$$

$$c_s = \sqrt{\frac{KT_e}{m_i}}, \quad (15)$$

$$\tau = T_i / T_e, \quad (16)$$

$$\kappa_n = \partial_r \ln n_0. \quad (17)$$

For the electrons, one can assume that the phase velocity of the instabilities is much lower than the electron thermal velocity. Moreover, electron-neutral collisions are considered at a collision rate ν_e . Consequently, kinetic effects are neglected, the electron distribution function is close to a Maxwellian, and a fluid model with an isothermal closure can be used. The model and calculations are the same as in Refs. 19 and 20. The electron response is

$$n_{e1} = n_{e0} \frac{\omega^* + i\nu_{\parallel}}{\omega - k_{\parallel} u_0 + i\nu_{\parallel}} \frac{e\phi}{KT_e} \quad (18)$$

with

$$\omega^* = k_{\theta} v_d = -k_{\theta} \frac{KT_e}{eB} \kappa_n, \quad (19)$$

the electron diamagnetic frequency, u_0 the electron drift parallel to the magnetic field,

$$v_d = -\frac{KT_e}{eB} \kappa_n, \quad (20)$$

the diamagnetic velocity, and

$$\nu_{\parallel} = \frac{k_{\parallel}^2 KT_e}{m_e \nu_e}. \quad (21)$$

Finally, Eq. (12) gives the following differential equation for $\phi(r)$:

$$\frac{d^2 \phi}{dr^2} + \left(\kappa_n + \frac{1}{r} \right) \frac{d\phi}{dr} + \left(Q(r) - \frac{m^2}{r^2} \right) \phi = 0 \quad (22)$$

with

$$Q(r) = \frac{J_0^2}{\rho_s^2} \left(\sum_{j=1}^M \alpha_j \frac{k_{\parallel}^2 c_s^2 - \frac{1}{\tau} \omega \Omega_j^*}{\omega^2 - k_{\parallel}^2 a_j^2} \right) - \frac{1}{\rho_s^2} \left(\frac{\omega^* + i\nu_{\parallel}}{\omega - k_{\parallel} u_0 + i\nu_{\parallel}} \right) \quad (23)$$

and $\rho_s^2 = \frac{c_s^2}{\Omega_e^2}$.

It is worth noting that the particular case $v_{\phi} \gg v_{T_i}$, i.e., $\omega \gg k_{\parallel} a_j, k_{\parallel} v_{T_i}$, and $J_0 = 1$, leads to the same expression as

the one obtained in Refs. 19 and 20 for drift waves, described by a fluid model and assuming $\nu_i = 0$

$$Q(r) = \frac{1}{\omega \rho_s^2} \left(\omega^* - \frac{\omega^* + i\nu_{\parallel}}{\omega - k_{\parallel} u_0 + i\nu_{\parallel}} \omega \right). \quad (24)$$

Moreover, the case $\nu_e = 0$ and $u_0 = 0$ leads to the same expression as the one obtained in Ref. 12 for ITG instabilities.

Finally, results of a comparison with a gyrofluid model are presented. The gyrofluid model is obtained by integrating the three first moments of the kinetic Eq. (1) and assuming a Maxwellian distribution function. In this case,

$$Q(r) = \frac{J_0^2 k_{\parallel}^2 v_{Ti}^2 \left(1 + \frac{2\Omega_n^* - \Omega_i^*}{\omega} \right) - \omega \Omega_n^*}{r_{Li}^2 (\omega^2 - 3k_{\parallel}^2 v_{Ti}^2)} - \frac{\tau}{r_{Li}^2} \left(\frac{\omega^* + i\nu_{\parallel}}{\omega - k_{\parallel} u_0 + i\nu_{\parallel}} \right) \quad (25)$$

with r_{Li} the ion Larmor radius, $\Omega_n^* = k_{\theta} \frac{KT_i}{qB} \kappa_n$ the ion diamagnetic frequency, $\Omega_i^* = k_{\theta} \frac{KT_i}{qB} \kappa_i$, and $\kappa_i = \partial_r \ln T_i$.

III. SPECTRAL METHOD

The ordinary differential Eq. (22) is of the form of the one studied in Ref. 15. In order to solve it in an efficient manner, we use the spectral method introduced in this article, which permits the computation of the "global" $\phi(r)$ profile. The function ϕ is expanded as follows:

$$\phi = \sum_{n=1}^N b_n f_n(r) \quad (26)$$

with N the total number of the functions f_n , chosen on the basis of an hypothesis of analyticity of ϕ , and fulfilling the boundary condition

$$\phi(a) = 0, \quad (27)$$

which states that there are no fluctuations at the edge of the machine. A good choice for f_n is

$$f_n(r) = r^m (a^2 - r^2) T_{2(n-1)}(r/a) \quad (28)$$

with m the azimuthal wavenumber.

For the discretization in r , we use collocation points defined by the N zeros of the Chebyshev polynomial $T_{2N}(r/a)$ that sit in the interval $[0, a]$, i.e.,

$$r_k = a \cos \left(\frac{(2k-1)\pi}{4N} \right) \quad (29)$$

for $k \in \{1, \dots, N\}$.

Equation (22) evaluated at these points yields the matrix problem

$$M(\omega)V = 0, \quad (30)$$

where $V = \begin{pmatrix} b_1 \\ \vdots \\ b_N \end{pmatrix}$ is the vector representing the solution

and $M(\omega)$ is a matrix.

Next, we scan the (ω_r, ω_i) plane, searching for values of ω such that one eigenvalue of the matrix $M(\omega)$ vanishes within machine precision. For this purpose, a method that finds the minimum of a scalar function of several variables, starting at an initial state, and uses the simplex search method,²¹ is used. Among these solutions, one finds the couple (ω_r, ω_i) for which the instability growth rate ω_i is maximum.

For a more detailed presentation of the method, the reader should refer to Ref. 15.

IV. ION TEMPERATURE GRADIENT INSTABILITIES

Here, we focus on the ability of the model to describe ITG instabilities for which an ion temperature gradient is needed. The parameter $\eta = \kappa_i / \kappa_n$, where $\kappa_i = \partial_r \ln T_i$ and $\kappa_n = \partial_r \ln n_0$, has to exceed a critical value^{22,23} to observe an ITG instability. This parameter can be increased either by flattening the density gradient or by increasing the ion temperature gradient. We focus here on the Columbia Linear Machine (CLM).^{5,6} CLM is a cylindrical device with radio-frequency heating employed to heat the core of the plasma column and produce a peaked ion temperature profile. Furthermore, the mesh for ion heating reduces the density in the central core and helps to reduce the density gradient. Therefore, this heating can produce high values of η . The goal is to compare the CLM experimental results⁶ with our global model. A hydrogen plasma with H_2^+ ions is produced in CLM. The magnetic field is $B = 0.1$ T. Typical plasma parameters are: $T_{e0} = 4$ eV, $T_{i0} = 9$ eV, $u_0 = 0.03 v_{Te}$, $k_{\parallel} = 2\pi/4.3$ m = 1.4 m⁻¹, and $m_i = 3.34 \times 10^{-27}$ kg.

Density and temperature profiles are approximated by

$$n_0(r) = n_{r_0} \exp \left[k_n r_n \tanh \left(\frac{r^2 - r_0^2}{r_n^2} \right) \right], \quad (31)$$

$$T_{\alpha}(r) = T_{\alpha 0} \exp \left[k_i r_i \tanh \left(\frac{r^2 - r_0^2}{r_i^2} \right) \right], \quad (32)$$

for $\alpha = e, i$.

The parameters $r_n = r_i = 1.6$ cm, $k_n = -13.9$ m⁻¹, and $k_i = -50$ m⁻¹, so that the profiles shown Fig. 3 are close to that measured in CLM. Moreover, for such a set of parameters, $\eta = \kappa_i / \kappa_n = k_i / k_n = 3.6$ is constant because $r_n = r_i$. The maximum value of r is the radius $a = 3.5$ cm of the device. $r = r_0$ is chosen to be $0.6 a$. The collision frequencies are approximately $\nu_e = 2.6 \times 10^6$ s⁻¹ (Ref. 24) and $\nu_i = 1.0 \times 10^4$ s⁻¹. For such parameters, the ratio of the destabilizing term of the linear instability growth rate of drift waves given by a fluid model (Eq. (18) in Ref. 15) due to the electron-neutral collisions over the stabilizing term due to ion-neutral collisions is greater than 15 with $m = 2$. Therefore, we can neglect ion-neutral collisions and their stabilizing effect,

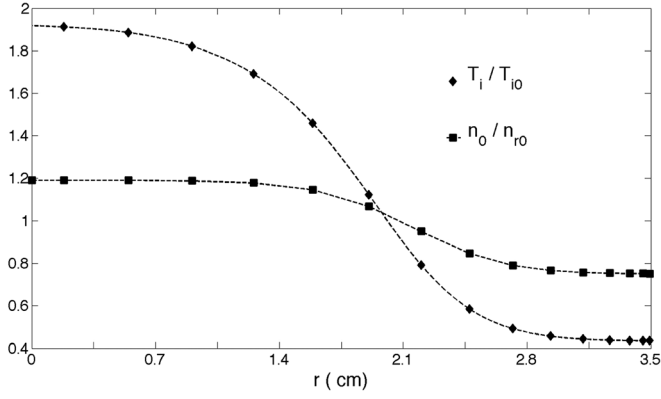


FIG. 3. Temperature (diamond) and density (square) normalized base profiles.

only electron-neutral collisions are taken into account and a water-bag distribution function can be chosen for ions.

The location $r = r_0$ is where temperatures are equal to T_{i0} or T_{e0} , the density $n_0 = n_{r_0}$, and where the reference water-bag distribution function is calculated. The construction of the water-bag distribution function (2) at this location is the same as in Ref. 12 for a Maxwellian distribution function

$$f_0(r, v_{\parallel}) = n_0(r) \sqrt{\frac{m_i}{2\pi K T_i(r)}} \exp\left[-\frac{m_i v_{\parallel}^2}{2K T_i(r)}\right]. \quad (33)$$

Thus, we assume that the WB distribution function at r_0 has been built and all $a_j(r_0)$ are known. Next, from this reference WB distribution function at r_0 , one has to build the water-bag distribution function as a function of r . We take into account the fact that all $A_j = F_j - F_{j+1}$ remain constant (Fig. 1), so that only the a_j is changing with radius. Calculating $F_j = f_0(a_j(r_0) - \Delta a(r_0)/2)$ and $F_{j+1} = f_0(a_j(r_0) + \Delta a(r_0)/2)$ at $r = r_0$, with $\Delta a(r_0)$ the constant step between two velocities $a_j(r_0)$ (see Ref. 12), and assuming that the F_j do not depend on r , one can write

$$\begin{aligned} \frac{F_j + F_{j+1}}{2} &= f_0(r, a_j) \\ &= n_0(r) \sqrt{\frac{m_i}{2\pi K T_i(r)}} \exp\left[-\frac{m_i}{2K T_i(r)} a_j^2(r)\right], \end{aligned} \quad (34)$$

hence

$$a_j(r) = \sqrt{-\frac{2K T_i(r)}{m_i} \ln \left[\frac{F_j + F_{j+1}}{2n_0(r)} \sqrt{\frac{2\pi K T_i(r)}{m_i}} \right]}, \quad (35)$$

Note that as a_j is a function of r , compared to Eq. (49) in Ref. 12, one must now take into account that $\Delta a_j = a_j(r) - a_{j-1}(r)$ depends on r . The coefficients γ_j/α_j , with $\alpha_j = 2a_j(F_j - F_{j+1})/n_0$, and γ_j such that Ref. 12

$$\alpha_j \Omega_j^* = \frac{1}{2} (\alpha_j - \gamma_j) \Omega_T^* + \gamma_j \Omega_n^*, \quad (36)$$

are now given by

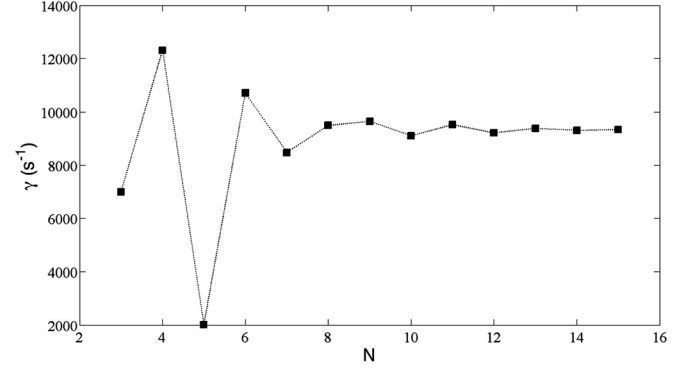


FIG. 4. In the case of Fig. 3, instability growth rate γ vs the number of coefficients N for a WB kinetic model ($M = 6$). The mode is $m = 2$, $\eta = 3.6$, and $u_0 = 0.03v_{Te}$.

$$\gamma_j/\alpha_j = \frac{1}{2a_j(F_j - F_{j+1})} [F_{j+1}\Delta a_j + F_j\Delta a_{j+1}]. \quad (37)$$

Equation (22) is solved using the spectral method with N the number of spectral basis functions, in the range,^{3,15} and the bag number $M = 6$. This number of bags is large enough for the model to converge toward the kinetic value of the linear instability growth rate.¹²

One can see (Fig. 4) that the instability growth rate converges rather rapidly as a function of N , here in the case of $m = 2$. In Fig. 5, where the b_n coefficients are presented, one can observe an exponential convergence. Hereafter, $N = 12$ will be used.

The mode with an azimuthal wavenumber $m = 2$ is the most unstable (Fig. 6), and an ITG instability with $\omega_r \sim -2.45 \times 10^4 \text{ s}^{-1}$ and $\gamma = \omega_i \sim 0.92 \times 10^4 \text{ s}^{-1}$ is observed. The angular frequency is negative, meaning that the perturbation propagates in the ion diamagnetic drift direction as expected for ITG instabilities.

With $T_i = 9 \text{ eV}$, the ion thermal velocity is equal to $2.1 \times 10^4 \text{ m s}^{-1}$, which is of the order of the ITG wave phase velocity, $v_{\phi} = -1.75 \times 10^4 \text{ m s}^{-1}$ since $k_{\parallel} = 1.4 \text{ m}^{-1}$. Wave-particle interaction effects can be expected. It is worth noting that the fluid model, which is not able to take into account the kinetic effects, indeed overestimates the instability growth rate by a factor 2 ($m = 2$ is also the fastest growing fluid

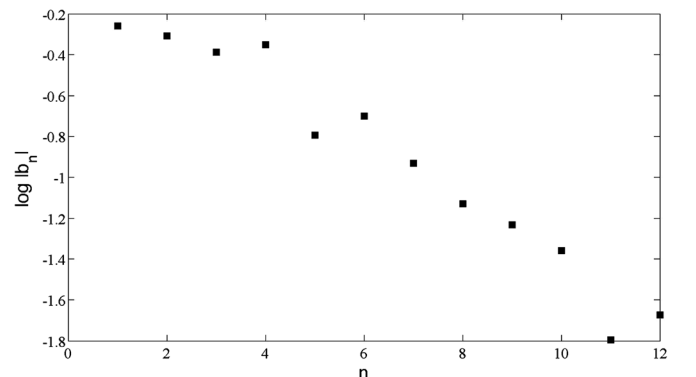


FIG. 5. Decimal logarithms of coefficients b_n vs n , for a computation with a total number of radial modes $N = 12$, with $\eta = 3.6$, $m = 2$ and with a WB kinetic model.

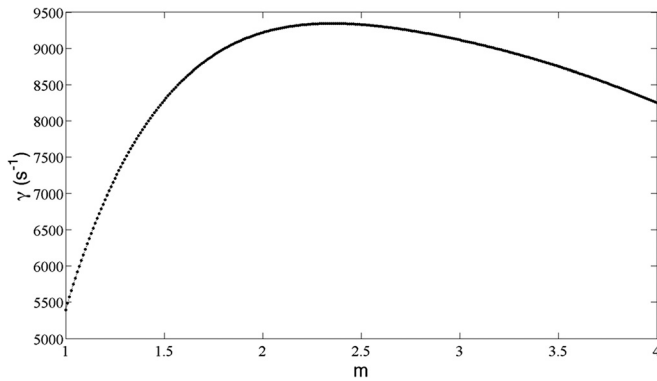


FIG. 6. In the case of Fig. 3, instability growth rate γ vs the azimuthal wave number m for a WB kinetic model ($M = 6$), $\eta = 3.6$ and $u_0 = 0.03v_{Te}$.

mode) when compared to the results presented here with the WB model, which is equivalent to a continuous kinetic model. This confirms that the kinetic phenomena play a stabilizing role when the thermal velocity is close to the phase velocity.

Also, in Fig. 7, the radial profile of the modulus of the wave plasma potential shows a maximum located where the temperature and density gradients are located.

The results presented are in a qualitative agreement with results obtained on the CLM device. The ITG mode is confirmed in the CLM device, where a $m = 2$ mode is obtained with a finite parallel wavelength and an azimuthal propagation in the ion diamagnetic drift direction. The angular frequency of this mode lies in the range $[3.7; 11.3] \times 10^4 \text{ s}^{-1}$, which is in agreement with our model prediction but slightly greater taking into account the fact that we did not look for being very close to the experimental profiles. The purpose is just to check that the most unstable mode is an ITG one, and that the value of the frequency is of the order of magnitude of the frequency measured experimentally.

V. COMPETITION BETWEEN DRIFT WAVES AND ION TEMPERATURE GRADIENT INSTABILITIES

The goal here is to study theoretically the transition from ITG to collisional drift waves instabilities when the parameter $|\kappa_t| = |\partial_r \ln T_i|$ decreases. When $|\kappa_t|$ (or η) becomes

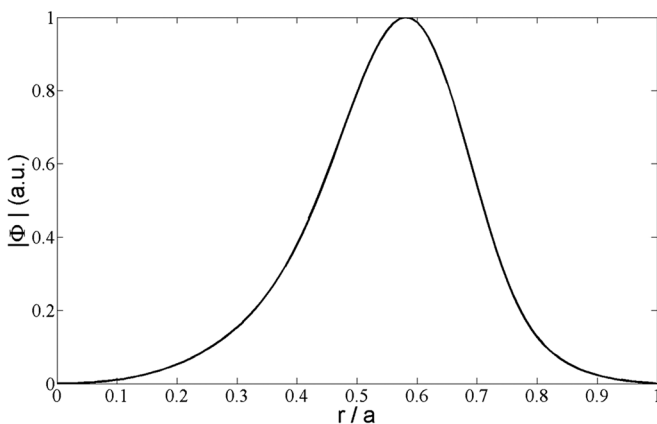


FIG. 7. Radial profile of the modulus of the wave plasma potential, for a computation with a total number of radial modes $N = 12$, with $\eta = 3.6$, $m = 2$ and with a WB kinetic model ($M = 6$).

smaller than a critical value, drift waves should be more unstable. The plasma parameters are the same as the ones of Sec. IV except for η being in the range $[2.1; 4.3]$: k_n is fixed to -13.9 m^{-1} and k_r is varied in the range $[-30; -60] \text{ m}^{-1}$. Note that in CLM, drift waves are not observed because of the low levels of κ_n and electron parallel drift u_0 ($u_0 \simeq 0.03v_{Te}$), which lead to a low drift wave instability growth rate when compared to that of the ITG instability. Concerning the destabilizing influence of u_0 , see, e.g., Ref. 15. In this section, in order to study the transition between drift waves and ITG, u_0 is taken to be $0.2v_{Te}$; this larger value may favour drift waves. Moreover, for such parameters, the destabilizing effect of electron-neutral collisions on drift waves is much greater than the stabilizing effect of ion-neutral collisions. Indeed using Eq. (18) in Ref. 15, the ratio is greater than 80 for $m = 2$. Therefore, here again ion-neutral collisions are neglected and a water-bag distribution function for ions can be considered.

Results are shown in Fig. 8. For η in the range $[2.16; 3.27]$, the linear growth rate is about $0.9 \times 10^4 \text{ s}^{-1}$ and corresponds to collisional drift waves with $m = 3$. ITG instability with $m = 3$ occurs if η exceeds the critical value $\eta = 3.27$, for which the ITG growth rate is greater than that of drift waves. The growth rate increases when η becomes larger, and a new transition is observed at $\eta = 3.55$ where an ITG instability with $m = 2$ occurs.

Note that the instability growth rates are smaller by a factor 2 when compared to the ones given by the fluid model. Moreover, using the fluid model, the bifurcation between drift waves $m = 3$ and ITG $m = 3$ instabilities takes place for $\eta = 2.66$, and the following bifurcation with $m = 2$ as the ITG fastest growing mode takes place for $\eta = 4.18$.

The angular frequency corresponding to the fastest growing mode is plotted against the parameter η in Fig. 9, in the case of the WB kinetic model. For $\eta < 3.27$, ω_r is greater than zero, the perturbation propagates in the electron diamagnetic drift direction as expected for drift waves. For $\eta > 3.27$, ω_r becomes negative, meaning that the perturbation propagates in the ion diamagnetic drift direction as expected for ITG instabilities. Note that the real frequencies are very close to the ones given by the fluid model.

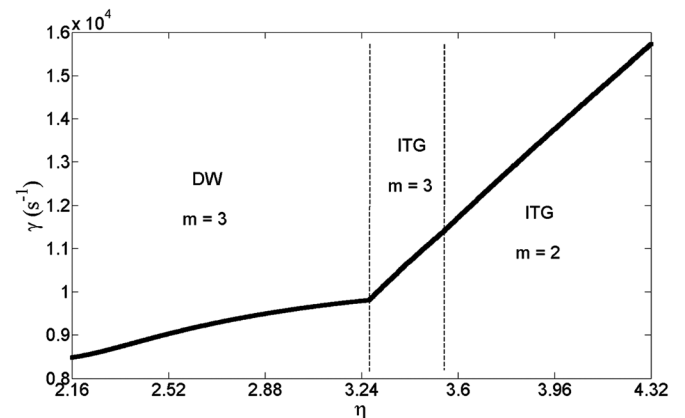


FIG. 8. Instability growth rate $\gamma_i = \omega_i$ of the fastest growing mode vs η given by the kinetic WB model.

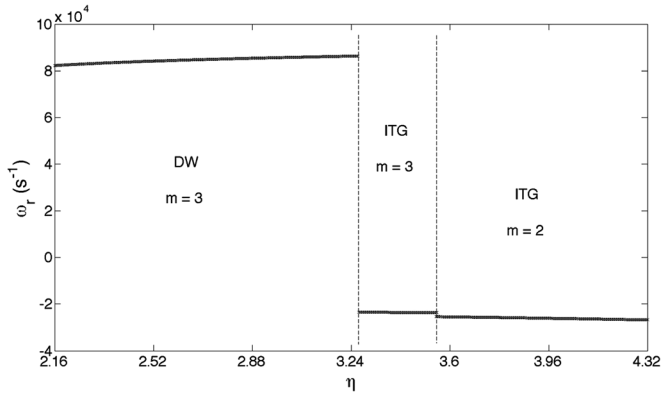


FIG. 9. Real frequencies ω_r of the fastest growing mode vs η given by the kinetic WB model.

The structure of the eigenmodes corresponding to the ITG mode $m = 3$ with $\eta = 3.54$ and the ITG mode $m = 2$ with $\eta = 3.56$ is shown in Figs. 10 and 11. The figures display both fluctuations of plasma potential in a section of the plasma column and the radial profile of the modulus of the wave plasma potential. The maximum of the fluctuations is located near the radius r_m at which $|\kappa_n|$ and $|\kappa_r|$ both attain their maximum value. Only a small change in the location of the maximum of the fluctuations between ITG $m = 3$ and ITG $m = 2$ modes is observed.

Moreover, it has been observed that the location of the maximum of the fluctuations for the drift wave (DW) mode $m = 3$ is the same as for the ITG mode $m = 3$ at $\eta = 3.27$.

This scenario between drift waves and ITG modes can be observed in any machine that allows one to vary significantly the parameter η . Our kinetic water-bag model seems to be well suited in order to describe such a transition.

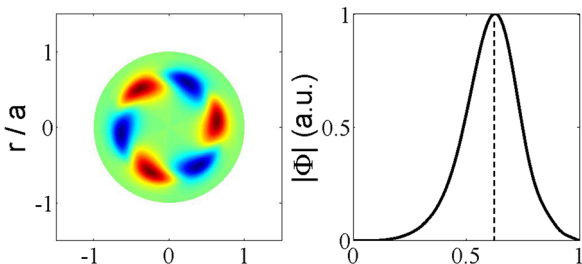


FIG. 10. ITG $m = 3$ fluctuations of plasma potential in a section of the plasma column (left) and radial profile of the modulus of the wave plasma potential (right) for $\eta = 3.54$. The dotted line shows the radius r_m at which $|\kappa_n|$ and $|\kappa_r|$ are maximum.

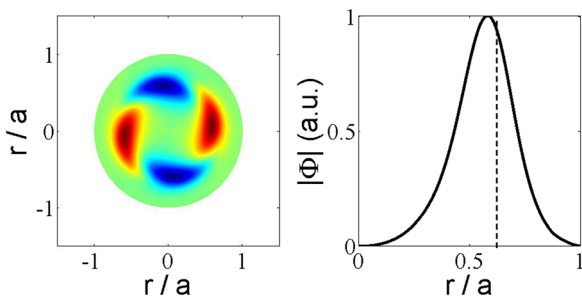


FIG. 11. Same as Fig. 10, but for an ITG wave $m = 2$ at $\eta = 3.56$.

VI. CONCLUDING DISCUSSION

Our model is able to describe simultaneously collisional drift waves and ITG instabilities. Interesting results have been obtained pointing to the ability of the collisional gyro-water-bag model to take into account kinetic effects for drift waves and ITG instabilities. Converting kinetic problems into multi-fluid ones, without a loss of generality, represents one interesting property of the multi-water-bag model.

The global model presented in this article is much more complete than the local one used in Ref. 13, because here radial boundary conditions are considered and the radial dependence of the eigenmodes is computed. This is rather easy with the new spectral method. This spectral method is accurate and suitable for numerical investigation of drift waves and ITG global modes in cylindrical geometry. It can be a very useful and fast tool to get the linear kinetic ITG or drift wave instability growth rates and to identify the fastest growing modes.

Moreover, as expected, the ITG instability depends strongly on the η parameter. It has been shown that a transition between drift waves and ITG instabilities appears as soon as η reaches a critical value, so that the ITG instability becomes dominant.

An interesting ability of the water-bag model is to allow the treatment of any distribution function: there is no constraint on the shape of the distribution function, which can be very far from a Maxwellian. This should permit, for instance, the study of the influence of energetic particles on ITG and drift wave instabilities.

ACKNOWLEDGMENTS

This work was carried out within the framework the European Fusion Development Agreement and the French Research Federation for Fusion Studies. The views and opinions expressed herein do not necessarily reflect those of the European Commission. Financial support was also received from the GYPSI (GYrokinetic high Performance Simulations for Iter) ANR contract. The authors wish to thank F. Hild for his helpful contribution during his Master 2 project at the Institute Jean Lamour of Nancy.

¹W. Horton, *Rev. Mod. Phys.* **71**, 735 (1999).

²X. Garbet, *Plasma Phys. Controlled Fusion* **43**, A251 (2001).

³L. Villard, S. J. Allfrey, A. Bottino, M. Brunetti, G. L. Falchetto, V. Grandgirard, R. Hatzky, J. Nührenberg, A. G. Peeters, O. Sauter, S. Sorge, and J. Vaclavik, *Nucl. Fusion* **44**, 172 (2004).

⁴T. Dannert and F. Jenko, *Phys. Plasmas* **12**, 072309 (2005).

⁵R. Scarmozzino, A. K. Sen, and G. A. Navratil, *Phys. Rev. Lett.* **57**, 1729 (1986).

⁶R. G. Greaves, J. Chen, and A. K. Sen, *Plasma Phys. Controlled Fusion* **34**, 1253 (1992).

⁷T. Klinger, A. Latten, A. Piel, G. Bonhomme, T. Pierre, and T. Dudok de Wit, *Phys. Rev. Lett.* **79**, 3913 (1997).

⁸E. Wallace, E. Thomas, A. Eadon, and J. Jackson, *Rev. Sci. Instrum.* **75**, 5160 (2004).

⁹M. Matsukuma, T. Pierre, A. Escarguel, D. Guyomarc'h, G. Leclert, F. Brochard, E. Gravier, and Y. Kawai, *Phys. Lett. A* **314**, 163 (2003).

¹⁰T. S. Hahm, *Phys. Fluids* **31**, 2670 (1988).

¹¹D. C. DePackh, *J. Electron. Control* **13**, 417 (1962).

¹²P. Morel, E. Gravier, N. Besse, R. Klein, A. Ghizzo, P. Bertrand, X. Garbet, P. Ghendrih, V. Grandgirard, and Y. Sarazin, *Phys. Plasmas* **14**, 112109 (2007).

- ¹³E. Gravier, R. Klein, P. Morel, N. Besse, and P. Bertrand, *Phys. Plasmas* **15**, 122103 (2008).
- ¹⁴R. Klein, E. Gravier, P. Morel, N. Besse, and P. Bertrand, *Phys. Plasmas* **16**, 082106 (2009).
- ¹⁵E. Gravier, E. Plaut, X. Caron, and M. Jenny, *Eur. Phys. J. D* **67**, 7 (2013).
- ¹⁶A. H. Boozer, *Rev. Mod. Phys.* **76**, 1071 (2005).
- ¹⁷F. R. Hansen, G. Knorr, J. P. Lynov, H. L. Pecseli, and J. J. Rasmussen, *Plasma Phys. Controlled Fusion* **31**, 173 (1989).
- ¹⁸V. Grandgirard, M. Brunetti, P. Bertrand, N. Besse, X. Garbet, P. Ghendrih, G. Manfredi, Y. Sarazin, O. Sauter, E. Sonnendrücker, J. Vaclavik, and L. Villard, *J. Comput. Phys.* **217**, 395 (2006).
- ¹⁹R. F. Ellis and E. Marden-Marshall, *Phys. Fluids* **22**, 2137 (1979).
- ²⁰R. F. Ellis, E. Marden-Marshall, and R. Majeski, *Plasma Phys.* **22**, 113 (1980).
- ²¹J. C. Lagarias, J. A. Reeds, M. H. Wright, and P. E. Wright, *SIAM J. Optim.* **9**, 112 (1998).
- ²²J. W. Connor and H. R. Wilson, *Plasma Phys. Controlled Fusion* **36**, 719 (1994).
- ²³R. J. Goldston and P. H. Rutherford, *Introduction to Plasma Physics* (IOP, London, 1995), pp. 468–469.
- ²⁴J. R. Roth, *Industrial Plasma Engineering* (IOP, London, 1995).